Oxygen isotope systematics of crystalline silicates in a giant cluster IDP: A genetic link to Wild 2 particles and primitive chondrite chondrules

Mingming Zhang[a*], Céline Defouilloy[a†], David J. Joswiak[b], Donald E. Brownlee[b], Daisuke Nakashima[a§], Guillaume Siron[a], Kouki Kitajima[a], Noriko T. Kita[a]

[a] *WiscSIMS, Department of Geoscience, University of Wisconsin–Madison, Madison, WI 53706, USA*

[b] *Department of Astronomy, University of Washington, Seattle, WA 98195, USA*

[*] *Corresponding address:* mzhang467@wisc.edu

[†] *Present address: Ingénieur Applications at CAMECA, 29 quai des Grésillons, 92633 Gennevilliers Cedex, France*

[§] *Present address: Department of Earth and Planetary Material Sciences, Tohoku University, Miyagi 980-8578, Japan*

Highlights

- Five out of 20 fragments (≥ 5 μm) in the giant cluster IDP U2-20GCA have chondrule-like textures.
- The oxygen isotope range and Mg#–$\Delta^{17}O$ relationship of crystalline silicate fragments are closest to Wild 2 particles and CR chondrite chondrules.
- Four fragments likely sourced from the formation regions of ordinary, R, or CH-CB chondrite chondrules.

ABSTRACT

Anhydrous interplanetary dust particles (IDPs) collected from Earth's stratosphere are the most primitive extraterrestrial materials that likely are the remnants of major building blocks of our solar system. While they probably originated from icy outer solar system comets, this hypothesis needs to be further verified via comparison with Wild 2 (a Jupiter-family comet) particles returned by the *Stardust* mission. Besides, the origins of their components can be further constrained by comparing with materials in primitive chondrite. Here we investigate the petrology and oxygen isotope systematics of 20 fragments extracted from a giant cluster IDP U2-20GCA. Fifteen are monomineralic or polymineralic fragments composed of olivine and/or pyroxene. Others are plagioclase/glass bearing fragments similar to barred-olivine chondrules, enstatite-rich chondrules, and Al-rich chondrules (ARC). They show a range of Mg# [mol% Mg/(Mg+Fe)] in olivine and pyroxene (99-75) and MnO and Cr_2O_3 abundances in olivine that resemble Wild 2 particles. Individual fragments have relatively ^{16}O-poor oxygen isotope ratios with $\delta^{18}O$ and $\delta^{17}O$ varying from –6.2 ± 1.0‰ to 6.8 ± 1.9‰ and –6.7 ± 2.6‰ to 5.3 ± 1.2‰, respectively. Most fragments show $\Delta^{17}O$ (= $\delta^{17}O$-0.52× $\delta^{18}O$) increasing from ~ –3‰ to ~ 0‰ with decreasing Mg#, similar to those observed in Wild 2 particles and CR chondrite chondrules. Four fragments (including the ARC-like fragment) show oxygen isotope signatures of ordinary (O), R, or CH-CB chondrite chondrules. The similarities among the giant cluster IDP, Wild 2 particles, and primitive chondrite chondrules demonstrate (i) a cometary origin of anhydrous IDPs; (ii) the major source of crystalline silicates in comets is likely to be CR chondrite chondrule-like materials, while minor sources include O, R, or CH-CB chondrite chondrule-like materials. The conclusions support the hypothesis that anhydrous IDPs sampled extremely heterogeneous materials formed in wide solar system regions like Wild 2 particles.

Keywords: giant cluster IDP; chondrule-like fragments; oxygen isotope ratios; Wild 2 particles; CR chondrite chondrules

1. Introduction

Interplanetary dust particles (IDPs, typically < 50 μm) collected from the Earth's stratosphere are among the most primitive extraterrestrial materials available for laboratory investigation (e.g., Bradley, 2014). They typically have chondritic elemental compositions and can be divided into (i) chondritic smooth, hydrated IDPs, compact objects dominated by hydrous minerals like cronstedtite, tochilinite, serpentine, saponite, etc.; (ii) chondritic porous, anhydrous IDPs, highly fluffy aggregates (up to 70% porosity) composed predominantly of submicron- to micron-sized olivine, pyroxene, iron-rich sulfide, Fe-Ni metal, glass with embedded metal and sulfide (GEMS), silicate glass, and carbonaceous material (Bradley, 2014). Refractory materials such as calcium-aluminum-rich inclusions (CAIs) and amoeboid olivine aggregates (AOAs) are rare (e.g., Joswiak et al., 2017). Some anhydrous IDPs contain abundant presolar grains, solar flare tracks typically in olivine or pyroxene, and unheated or only slightly heated carbonaceous materials, suggesting that they suffered minimal mineralogical modifications during atmospheric entry (peak temperature typically < 100 °C) (Matrajt et al., 2012; Bradley, 2014). The atmospheric entry velocity is inferred to be slow, consistent with an origin from asteroids or comets with low inclinations and perihelia larger than 1.2 astronomical units (Sandford and Bradley, 1989).

Wild 2 (a Jupiter-family comet) particles returned by the NASA *Stardust* mission in 2006 provide important insights into the mineralogy, chemistry, and isotope geochemistry of outer solar system cometary materials. The most striking findings are high-temperature objects similar to inner-disk CAIs and chondrules (Zolensky et al., 2006; Nakamura et al., 2008; Bridges et al., 2012; Ogliore et al., 2012; Gainsforth et al., 2015; Joswiak et al., 2017), strongly demonstrating large-scale transportation of solids across the full dimension of the protoplanetary disk (Brownlee, 2014). Like anhydrous IDPs, Mg# [mol% Mg/(Mg+Fe)] of olivine and pyroxene in Wild 2 particles are evenly distributed from 100 to 58, Fe vs. Mn abundances of olivine span a wide range that do not follow the trendlines defined by CO and ordinary (O) chondrite chondrules, suggesting a diversity of source regions for these particles (Zolensky et al., 2006; Berlin et al., 2011; Frank et al., 2014; Brownlee and Joswiak, 2017). Oxygen isotope ratios of Wild 2 particles have been determined by Secondary Ion Mass Spectrometry (SIMS) that show solar-like ^{16}O-rich compositions ($\delta^{18}O \sim -50$ ‰) and chondrule-like ^{16}O-poor compositions ($\delta^{18}O \sim -6$‰ to +7‰) (McKeegan et al., 2006; Nakamura et al., 2008; Bridges et al.,

2012; Nakashima et al., 2012a; Gainsforth et al., 2015; Ogliore et al., 2015; Defouilloy et al., 2017). The majority of these SIMS data were obtained from coarse (4-30 μm) particles using a CAMECA IMS-1280 and a ~2 μm beam with a precision in $\Delta^{17}O$ of ~2‰. In particular, Nakashima et al. (2012a) and Defouilloy et al. (2017) studied olivine and pyroxene bearing particles and revealed a systematic change in mass-independent fractionation of oxygen isotopes ($\Delta^{17}O = \delta^{17}O - 0.52 \times \delta^{18}O$) with their Mg# values similar to CR chondrite chondrules.

Oxygen isotope ratios of anhydrous IDPs have been determined mostly by NanoSIMS on nm-scale tiny minerals or their mixtures that represent diverse components in the early solar system, including extremely ^{16}O-rich presolar grains ($\delta^{18}O$ down to –160‰), solar-like ^{16}O-rich or chondritic-like ^{16}O-poor objects ($\delta^{18}O$ = –30‰ to +19‰), and significantly ^{16}O-poor objects ($\delta^{18}O$ = +80‰ to +200‰) that likely formed by isotope self-shielding in the outer solar system (e.g., Busemann et al., 2009; Starkey et al., 2014). Compared to Wild 2 particles, high-precision oxygen isotope data of anhydrous IDPs are limited due to the lack of suitable large fragments (> 2 μm) for higher precision SIMS analyses. Crystalline silicates in three anhydrous IDPs show chondrule-like ^{16}O-poor isotope ratios, with average $\delta^{18}O$ ranging from –2.9 ± 0.7‰ to 1.0 ± 2‰ (Aléon et al., 2009; Nakashima et al., 2012b). Thus, new high-precision oxygen isotope data of anhydrous IDPs are needed for better comparison with Wild 2 particles and primitive chondrite components in order to verify the cometary origin of anhydrous IDPs and elucidate the sources of their crystalline silicates.

A giant cluster IDP U2-20GCA, collected by impact onto a silicone oil-coated substrate flag "U2-20" in the stratosphere, was utilized in this study. It is an extremely porous and fragile object composed of a ~ 350 μm core surrounded by a ~ 1 mm low-density debris halo, where the core is made up of a dense monolayer of thousands of dark and transparent fragments (up to 42 μm) (Joswiak et al., 2017). CAIs, AOAs, and "Kool grains" (kosmochloric Ca-rich pyroxene + Fe-rich olivine ± Cr-rich spinel ± aluminosilicate glass or albitic feldspar) have been found in the giant cluster IDP in addition to other common anhydrous IDP components (Joswiak et al., 2009; Matrajt et al., 2012; Joswiak et al., 2017). Large (> 5 μm) crystalline silicate fragments were extracted from the giant cluster IDP and high-precision oxygen isotope ratios were determined. However, the fine-grained fraction of the giant cluster IDP has not been studied here, and thus, the sources inferred from oxygen isotope ratios of large fragments may not represent the whole giant cluster IDP.

2. Analytical procedures

2.1. Sample preparation

Twenty large crystalline silicate fragments from the giant cluster IDP were extracted under an optical microscope with a glass needle and washed with hexane to remove surface silicone oil (Joswiak et al., 2017). The following sample preparation procedures are similar to those for Wild 2 particles previously described by Joswiak et al. (2012), Nakashima et al. (2012a), and Defouilloy et al. (2017). The fragments were first embedded into acrylic or epoxy cylinders for ultramicrotomy. Typically, 70-100 nm thick microtome sections were made using a 45° diamond knife on a Leica Ultracut S ultramicrotome. The sections were then transferred onto 200 mesh Cu or Au transmission electron microscope (TEM) grids coated with 10 nm thick carbon films for TEM examination. The remaining portion of each fragment known as a "potted butt" was removed as a 100 μm cube and pressed into a 1.4 mm diameter indium metal located at the center of an 8 mm or 25 mm aluminum disk for SIMS analysis. A polished San Carlos olivine (SC-Ol) grain was pressed within 500 μm of the sample fragments to serve as a SIMS running standard. The topography of sample surroundings was checked using a ZYGO NewView white light profilometer at the University of Wisconsin-Madison (UW-Madison), demonstrating that height differences are typically < 3 μm.

2.2. Electron microscopy

The microtome sections on TEM grids were placed in a double-tilt beryllium sample holder and studied using a field emission scanning transmission electron microscope (Tecnai TF20 STEM) at the University of Washington. The STEM is equipped with bright-field and dark-field CCD cameras, a secondary electron (SE) detector, and a high-angle annular dark-field scanning TEM detector. The analytical procedures are similar to those described by Joswiak et al. (2009) and Joswiak et al. (2012). Secondary electron and/or backscattered electron (BSE) images of the potted butts were obtained using a field emission scanning electron microscope (FE-SEM; JEOL JSM 7000F) at the University of Washington or a conventional tungsten-sourced SEM (Hitachi S3400) at the UW-Madison. These images were taken under low electron doses with minimal beam exposure time to minimize electron damage and shrinkage of acrylic resins that could affect sample topography. In order to improve the accuracy of aiming during SIMS analysis, the candidate positions were

marked by removing a 1×1 um square of surface carbon (20-30 nm thick) using a focused ion beam SEM (FIB-SEM; Zeiss Auriga) at the UW-Madison. The carbon coatings were efficiently removed without damaging the fragments after 90 s sputtering using a focused Ga^+ ion beam with an acceleration voltage of 30 keV and a beam current of 5 pA (Nakashima et al., 2012a; Defouilloy et al., 2017).

2.3. Oxygen-three isotope analysis

Oxygen isotope ratios of 20 fragments from the giant cluster IDP were determined using the CAMECA IMS 1280 at the WiscSIMS laboratory of UW-Madison. Measurements were obtained in five separate sessions. The analytical conditions and procedures for all sessions were generally similar and have been described in detail in Nakashima et al. (2012a) and Defouilloy et al. (2017). The Cs^+ primary beam was focused to ~ 2×1.5 μm^2 with an intensity of 2.5-3 pA. The analysis positions were located via FIB marks, which appear as bright spots (no carbon coating) on the $^{16}O^-$ ion image generated by rastering a 10×10 μm^2 square. Centering FIB marks to the ion image was achieved by first adjusting the sample stage by ≥ 1 μm steps and then, except for the Nov. 2011 session, shifting the beam position by ≥ 0.1 μm steps using the "NanoDeflector" system developed in the WiscSIMS laboratory (Defouilloy et al., 2017). Secondary ions $^{16}O^-$, $^{17}O^-$, and $^{18}O^-$ were detected simultaneously using a Faraday cup ($^{16}O^-$) with 10^{11} Ω resistance (except for the Oct. 2017 session which used 10^{10} Ω) and two electron multipliers ($^{17}O^-$ and $^{18}O^-$). The count rate of $^{16}O^-$ was 1-3×10^6 cps (counts per second). The mass resolving power (MRP) was set to ~ 6000 for axis detector (^{17}O) and the contribution of tailing $^{16}O^1H^-$ ions on the $^{17}O^-$ signals was negligible (typically < 1‰ correction). Each analysis required ~ 25 min (including 20 cycles of acquisition of 60 s each), giving average internal precisions (2SE) of 1.2 ‰, 2 ‰, and 2‰ for $\delta^{18}O$, $\delta^{17}O$, and $\Delta^{17}O$, respectively. Depending on the number and size of fragments on a single mount, blocks of 1-7 analyses of sample fragments were bracketed by 6-8 analyses on the nearby SC-Ol standard. The external reproducibility (2SD) on the SC-Ol standard was typically 1.5‰, 2‰, and 1.7‰ for $\delta^{18}O$, $\delta^{17}O$, and $\Delta^{17}O$, respectively; therefore, very similar to the 2SE of individual analysis. For fragments that show indistinguishable oxygen isotope ratios among multiple analyses, mean values were calculated. The uncertainties of mean values are propagated from (i) the maxima of the 2SD of multiple sample analyses versus the 2SD of bracketing standard analyses; (ii) 2SE (standard error of the mean) of

147 instrumental bias calculated from 6-8 bracket standard analyses; (iii) external reproducibility for instrumental
148 bias correction across a 1 mm center area of an 8 mm disk (0.5‰ in $\delta^{18}O$ 0.25‰ in $\delta^{17}O$) (Nakashima et al.,
149 2012a; Defouilloy et al., 2017). If only one analysis was made for a fragment, we propagated uncertainties
150 from (ii) and (iii) to the final value. At the beginning of or during each session, multiple standards of olivine
151 (Fo_{100}, Fo_{82}, Fo_{73}, Fo_{60},), orthopyroxene (En_{99}, $En_{96.3}$, En_{85}, En_{70}), diopside (pure $CaMgSi_2O_6$), and/or glass
152 (SiO_2: 63.7 wt% and 76 wt%) were analyzed and bracketed by SC-Ol analyses (Supplementary S1 Table S1).
153 Instrumental biases of olivine, pyroxene, and mesostasis in the sample fragments were corrected as a function
154 of Fo, En, Wo, and SiO_2 contents (Supplementary S1 Table S2). After each session, the locations and
155 morphology of SIMS pits were examined under similar imaging conditions on the conventional SEM and FIB-
156 SEM at the UW-Madison (Supplementary S2).

157 # 3. Results

158 ## *3.1. Petrology*

159 The 20 fragments were extracted from the largest grain size fraction of the giant cluster IDP. Their
160 longest dimensions range from 5 μm to 35 μm, eight larger than 10 μm in both length and width. They are
161 mostly monomineralic (6/20) or polymineralic (9/20) fragments consisting of olivine and/or pyroxene (Table 1;
162 Figs. 1a, 1b, 1c). Sulfide is rare. Four fragments have chondrule-like mineral assemblages: (i) LT24 is
163 composed mainly of enstatite with minor amounts of feldspar (An_{57}), augite, and crystalline silica (Fig. 1d); (ii)
164 LT11 consists of enstatite, feldspathic glass/feldspar, and minor kamacite, schreibersite [$(Fe, Ni)_3P$], and
165 pyrrhotite (Fig. 1e); and (iii) LT17 and LT23 have barred-olivine textures composed of olivine bars, chromite,
166 and mesostasis (Figs. 1f, 1g), of which LT17 has two sets of olivine bars that are almost perpendicular. LT410
167 is composed mainly of forsterite with minor anorthite and Al-diopside (Fig. 1h), with a mineral assemblage
168 similar to AOAs and Al-rich chondrules (ARC).

169 Olivine in 13 fragments shows a compositional range from Fo_{75} to Fo_{99}; eleven are iron-rich (Fo_{75-86})
170 and two are forsteritic (Fo_{99}) (Table 1). Iron-rich olivines contain minor abundances of MnO (0.20-0.54 wt%)
171 and Al_2O_3 (0-0.47 wt%) but nearly free of Cr_2O_3 (≤ 0.12 wt%). In contrast, forsteric olivines are richer in
172 Cr_2O_3 (0.67-0.74 wt%) but poorer in MnO (0.11-0.18 wt%) and free of Al_2O_3. CaO content in olivine varies

from 0.14 wt% to 0.88 wt% and is independent of their Mg# values. Pyroxene in 13 fragments is enstatite (6/13), pigeonite (6/13), or augite (1/13). Enstatite is richer in MgO ($En_{90-98}Wo_{\leq 3.2}$) but poorer in Al_2O_3 (≤ 2.15 wt%) compared to pigeonite ($En_{72-75}Wo_{5-9}$; Al_2O_3=1.82-5.17 wt%) and augite ($En_{73}Wo_{18;}$ Al_2O_3=3.04 wt%). Enstatite and augite have higher abundances of Cr_2O_3 (0.84-1.18 wt% vs. ≤ 0.61 wt%) and MnO (0.15-1.33 wt% vs. ≤ 0.45 wt%) than pigeonite. Pigeonite generally intergrows with iron-rich olivine (Fig. 1c) and shows similar Mg# values, except LT14 (Fo_{78} vs. En_{97}). TiO_2 and Na_2O contents in pyroxene are low, i.e., ≤ 0.77 wt% and ≤ 0.25 wt%, respectively. Mesostasis in the two BO chondrule-like fragments (LT17 and LT23) is SiO_2-rich (>70 wt%) and contains < 11 wt% MgO, < 7 wt% FeO, < 13 wt% Al_2O_3, and < 1 wt% Na_2O.

3.2. Oxygen isotopes

A total of 73 analyses were performed on olivine (34/73) and pyroxene (39/73) of the 20 fragments in the giant cluster IDP (Supplementary S1 Table S2). Two analysis points on fragment LT7 (LT7#1, #2) have significantly higher OH^- intensities (up to 3.7×10^5 cps) than other points on the same fragment (typically ~ 1×10^3 cps), likely indicating a severe overlap with the surrounding epoxy resin and therefore were rejected. The oxygen isotope ratios among multiple analyses on a monomineralic fragment or olivine and pyroxene of a polymineralic fragment are homogeneous, with their 2SD typically smaller than or very similar to those of the running standard SC-Ol. Thus, only mean oxygen isotope ratios for each fragment were used in the following illustrations and discussions. The 20 fragments have mean $\delta^{18}O$, $\delta^{17}O$, and $\Delta^{17}O$ ranging from –6.1 ± 0.9‰ to 5.7 ± 1.1‰, –6.4 ± 2.1‰ to 5.2 ± 1.2‰, and–3.2 ± 2.0‰ to 3.4 ± 1.5‰, respectively (Table 2). The four chondrule-like fragments (LT11, LT17, LT23, and LT24) have oxygen isotope ratios similar to other monomineralic/polymineralic fragments, with mean $\delta^{18}O$, $\delta^{17}O$, and $\Delta^{17}O$ varying from –0.1 ± 1.2‰ to 3.0 ± 1.1‰, –2.4 ± 1.4‰ to 0.7 ± 0.9‰, and–2.4 ± 1.6‰ to –0.8 ± 1.0‰, respectively. The AOA/ARC-like fragment LT410 has $\delta^{18}O$, $\delta^{17}O$, and $\Delta^{17}O$ of –2.1 ± 1.3‰, –2.5 ± 1.7‰, and –1.4 ± 1.4‰, respectively. $\Delta^{17}O$ values of these fragments show a negative correlation with their Mg# values, i.e., Mg# > 97 fragments have $\Delta^{17}O$ of –3.2 ± 2.0‰ to –0.9 ± 1.8‰, Mg# = 80-97 fragments have $\Delta^{17}O$ of –3.1 ± 2.2‰ to 1.9 ± 1.4‰, and Mg# = 70-80 fragments have $\Delta^{17}O$ of –0.8 ± 1.0‰ to 3.4 ± 1.5‰. In the diagram of $\delta^{18}O$ vs. $\delta^{17}O$ (Fig. 2), oxygen isotope ratios of most fragments are scattered on the primitive chondrule mineral (PCM) line

(Ushikubo et al., 2012) and the Young & Russell (Y&R) line (Young and Russell, 1998), while three fragments (LT7, LT14, and LT400) plot above the terrestrial fractionation (TF) line. $\delta^{18}O$ vs. $\delta^{17}O$ diagrams for individual fragments are shown in Figs. S2-S4.

4. Discussion

4.1. Petrology comparison of anhydrous IDPs with Wild 2 particles and primitive chondrite chondrules

While hydrothermal alteration has been detected rarely in anhydrous IDPs and Wild 2 particles (e.g., Hicks et al., 2017), it is acknowledged that they are dominated by anhydrous phases/assemblages like olivine, pyroxene, Fe-Ni metals, Fe-Ni sulfides, CAIs, and AOAs (Bradley, 2014; Brownlee, 2014; Joswiak et al., 2017), which are common components in most primitive chondrites. Kool grains, a unique mineral assemblage identified in anhydrous IDPs and Wild 2 particles, are thought to be the precursor of iron-rich chondrules in ordinary chondrites, though it has not been observed in any chondrites (Joswiak et al., 2009). However, enstatite whiskers/platelets, presolar grains, GEMS, carbon, and aromatic compounds that are abundant or common in anhydrous IDPs appear to be rare or absent in Wild 2 particles (e.g., McKeegan et al., 2006; Ishii et al., 2008; Stodolna et al., 2012), which is in part due to the alteration of fine-grained and volatile materials during the collection of Wild 2 particles at a high impact velocity (~6.1 km/s) (Brownlee, 2014). Similarly, these materials could easily be destroyed during thermal metamorphism and metasomatism events on their parent bodies, resulting in extreme heterogeneity in abundances and species among different chondrites (e.g., Nittler et al., 2019).

Olivine and pyroxene in anhydrous IDPs and Wild 2 particles span a similar Mg# range from 100 to 58 without pronounced frequency peaks, in contrast to olivine Mg# in both chondrules and matrix in most chondrite groups that typically have peak(s) of distributions at >90 and/or 50-80 (Zolensky et al., 2006; Berlin et al., 2011; Frank et al., 2014). Unlike typical anhydrous IDPs, the Mg# of olivines and pyroxenes in the 20 fragments of the giant cluster IDP show a bimodal distribution at >90 and 75-80. This is similar to CR chondrite chondrules that have a strong peak at >90 (Frank et al., 2014) and may have a second peak at ~71 for Type II chondrules (Berlin et al., 2011). Fe-Mn systematic of olivines in anhydrous IDPs and Wild 2 particles

are significantly overlapped with those of CR chondrite chondrules, but nearly cover the entire range of the chondrule data including those from CO and O chondrites; therefore, these olivines are likely from regions of CR, CO, and O chondirte chondrules instead of a single source (Brownlee and Joswiak, 2017). Fe vs. Mn in olivines in the giant cluster IDP fall in the ranges of anhydrous IDPs, Wild 2 particles, and CR chondrite chondrules. It is noteworthy that fragment LT14, whose olivine and pyroxene appear to be unequilibrated, has an elevated Mn content that plots close to the correlation line defined by O chondrite chondrules (Fig. 3). Like Wild 2 particles, iron-rich olivines in the giant cluster IDP have Cr_2O_3 ($\leq$ 0.12 wt%) abundances lower than primitive CO, CR, and O chondrite chondrules (Fig. 4), which may indicate mild thermal metamorphism (petrologic type 3.05-3.15 when compared with O chondrites and >3.1 when compared with CO chondrites) (Frank et al., 2014). This low Cr_2O_3 content in olivine could also result from chromite precipitation before or concurrently with olivine (Gainsforth et al., 2015). In addition, pigeonite in the giant cluster IDP typically occurs as a single crystal intergrown with iron-rich olivine instead of a discrete, intermediate layer between low-Ca pyroxene and augite overgrowth like in Type II chondrules of O chondrites (Brearley and Jones, 1998), likely suggesting a carbonaceous chondirte source.

One of the important findings from Wild 2 particles is the identification of chondrule-like fragments (e.g., Nakamura et al., 2008; Gainsforth et al., 2015), while similar objects have rarely been reported among single anhydrous IDPs. This finding contrast with the five chondrule-like fragments observed out of 20 fragments in the giant cluster IDP. LT11 and LT24 are composed mainly of enstatite with minor feldspathic glass/feldspar ± augite ± crystalline silica ± kamacite ± schreibersite ± pyrrhotite (Figs. 1d, 1e), resembling the porphyritic pyroxene (PP) chondrules. Similar objects such as "Gen-chan," "Lily," and "Pyxie" have been reported in Wild 2 particles (Nakamura et al., 2008; Nakashima et al., 2012a). LT17 and LT23 have typical barred-olivine textures consisting of iron-rich olivine bars (Fo_{75-86}), SiO_2-rich mesostasis (> 70 wt%), and chromite inclusions (Figs. 1f, 1g), resembling the iron-rich BO chondrules. Similar objects have not been found in Wild 2 particles. LT410 comprises forsterite ($Fo_{99.2}$), Al-diopside, and anorthite (Fig. 1h) with a mean $\Delta^{17}O$ of –1.4 ± 1.4‰, confirming that it is an ARC-like fragment. A similar ARC-like particle ("Bidi") has been reported in the *Stardust* track 130, composed of forsterite (Fo_{97}), anorthite (An_{97}), and Al-Ti-bearing clinopyroxene with a mean $\Delta^{17}O$ of –2.2 ± 2.0‰ (Joswiak et al., 2014). In summary, the Mg# distribution, Fe-

Mn systematics of olivine, Cr_2O_3 abundance in olivine, and mineral assemblages of chondrule-like fragments, in anhydrous IDPs (including the giant cluster IDP) are almost indistinguishable from Wild 2 particles. Similarities in the first two factors may indicate a genetic relationship to CR chondrite chondrules.

4.2. Oxygen isotope systematic comparison of anhydrous IDPs with Wild 2 particles and primitive chondrite chondrules

Limited high-precision oxygen isotope data of olivine and low-Ca pyroxene in anhydrous IDPs show chondrule-like ^{16}O-poor compositions, with average $\delta^{18}O$, $\delta^{17}O$, and $\Delta^{17}O$ ranging from –2.9 ± 0.7‰ to 1.0 ± 2‰, –5.8 ± 0.8‰ to –1.3 ± 1.8‰, and –4.3 ± 0.9‰ to –1.8 ± 2.2‰, respectively (Aléon et al., 2009; Nakashima et al., 2012b). New oxygen isotope data of 20 crystalline silicate fragments in the giant cluster IDP indicate similar chondrule-like ^{16}O-poor compositions but span a wider range, with average $\delta^{18}O$, $\delta^{17}O$, and $\Delta^{17}O$ varying from –6.2 ± 1.0‰ to 6.8 ± 1.9‰, –6.7 ± 2.6‰ to 5.3 ± 1.2‰, and –5.2 ± 2.6‰ to 3.4 ± 1.5‰, respectively (Table 2). The range of oxygen isotope ratios is slightly narrower than the ^{16}O-poor silicates in Wild 2 particles ($\delta^{18}O$: –12.2 ± 1.8‰ to 7.2 ± 1.6‰; $\delta^{17}O$: –13 ± 2.0‰ to 5.5 ± 2.8‰; $\Delta^{17}O$: –6.9 ± 4.2‰ to 2.4 ± 2.8‰; Fig. 2) (Nakamura et al., 2008; Nakashima et al., 2012a; Joswiak et al., 2014; Ogliore et al., 2015; Defouilloy et al., 2017) but similar to the CR chondrite chondrules ($\delta^{18}O$: –6.4 ± 0.4‰ to 7.3 ± 0.4‰; $\delta^{17}O$: –9.5 ± 0.8‰ to 3.8 ± 0.5‰; $\Delta^{17}O$: –6.3 ± 1.1‰ to 1.1 ± 0.7‰; Fig. 5) (Connolly and Huss, 2010; Schrader et al., 2013; Schrader et al., 2014; Tenner et al., 2015). LT11 ($\Delta^{17}O$ = –0.9 ± 1.8 ‰) and LT24 ($\Delta^{17}O$ = –2.3 ± 1.4 ‰) in the giant cluster IDP have nearly identical oxygen isotope ratios to similar PP chondrule-like particles "Pyxie" ($\Delta^{17}O$ = –1.1 ± 0.9 ‰) and "Gen-chan" ($\Delta^{17}O$ = –2.3 ± 1.4 ‰) in *Stardust* tracks (Nakamura et al., 2008; Nakashima et al., 2012a). PP chondrules in CR and CV/CO/CM/Acfer 094 chondrites have negative $\Delta^{17}O$ values (~ –6‰ to ~ 0‰ and ~ –7‰ to ~ –2‰, respectively; Ushikubo et al., 2012; Tenner et al., 2013; Tenner et al., 2015; Chaumard et al., 2018; Hertwig et al., 2018), while similar objects in O and enstatite (E) chondrites have positive $\Delta^{17}O$ values (~ 0‰ to ~ 2‰; Kita et al., 2010; Weisberg et al., 2011). LT17 ($\Delta^{17}O$ = –2.4 ± 1.6‰) and LT23 ($\Delta^{17}O$ = –0.8 ± 1.0‰) have oxygen isotope ratios similar to iron-rich BO chondrules in CR and CO chondrites ($\Delta^{17}O$: ~ –2‰ to ~ 0‰; Connolly and Huss, 2010; Tenner et al., 2013; Schrader et al., 2014). Thus, the four chondrule-like fragments (LT11, LT24, LT17, and LT23) are likely related to

carbonaceous chondrite (except CH-CB) chondrules. In contrast, the ARC-like fragment LT410 ($\Delta^{17}O$ = –1.4 ± 1.4‰) is relatively ^{16}O-poor compared to ARCs in CV/CO/Acfer 094 chondrites ($\Delta^{17}O$ ~ –5‰) (e.g., Zhang et al., 2020) but falls in the ranges of ARCs in O, CR, and CH chondrites ($\Delta^{17}O$: –8‰ to +4‰) (e.g., Krot et al., 2017), suggesting an origin similar to the latter.

For the mono/polymineralic fragments in the giant cluster IDP, LT7 and LT14 plot within regions of O and R chondrite chondrules, LT400 plots close to the R or CH-CB chondrite chondrules, and the others plot within the ranges of CR and CV/CO/CM/Acfer 094 chondrite chondrules (Fig. 5). This comparison suggests that most fragments have an origin of carbonaceous chondrite chondrules (except CH-CB), and few have origins of O, R, or CH-CB chondrite chondrules. The possible O chondrite origin of LT14 is consistent with the high MnO content in its iron-rich olivine plotting close to the line defined by O chondrite chondrules (Fig. 3). Moreover, LT14 is in chemical disequilibrium composed of iron-rich olivine (Fo_{78}) and magnesium-rich enstatite (En_{97}) and suggests that olivine underwent Fe-Mg exchange during mild thermal metamorphism on the O/R-like chondirte parent body. In contrast, enstatite remains intact due to a lower Fe-Mg interdiffusion rate (Ganguly and Tazzoli, 1994).

$\Delta^{17}O$ of crystalline silicate fragments in the giant cluster IDP appears negatively-correlated with their Mg# values, where $\Delta^{17}O$ of Mg# > 90 fragments typically cluster around –3‰, and their $\Delta^{17}O$ gradually increases to ~ 0‰ as Mg# decreases from 90 to 80 and finally cluster around 0‰ in Mg# = 75-80 fragments (Fig. 6a). As exceptions, LT14 and LT400 deviate from the Mg#–$\Delta^{17}O$ trend, consistent with their O, R, or CH-CB origins; however, LT7 and LT410 plot on this trend. For the remaining fragments, the Pearson correlation coefficient for their $\Delta^{17}O$ and Mg# is –0.74, indicating that the two parameters are negatively correlated. The Mg#–$\Delta^{17}O$ trend of the giant cluster IDP is very similar to the ^{16}O-poor Wild 2 particles, i.e., Mg# > 97 particles have $\Delta^{17}O$ of ~ –2‰ and Mg# < 97 particles have $\Delta^{17}O$ varying from –4‰ to +2‰ (Fig. 6b). To quantify the similarity of Mg#–$\Delta^{17}O$ relationship between crystalline silicates in the giant cluster IDP and Wild 2 particles, a two samples Kolmogorov–Smirnov (K-S) test for two variables (Mg# and $\Delta^{17}O$) was performed. This test compares the cumulative distributions of two datasets and returns a *p*-value representing a probability that the two datasets belong to the same distribution. The K-S test returns a *p*-value of 0.28 for

crystalline silicates in the giant cluster IDP and Wild 2 particles, indicating that they are likely from the same population.

On the other hand, the Mg#–Δ^{17}O correlation in the giant cluster IDP allows for comparing with those in primitive chondrite chondrules and then elucidating the genetic relationships (Fig. 6). While the crystalline silicate fragments in the giant cluster IDP might have formed via high-temperature annealing (~1000 K) in the inner solar system (Nuth et al., 2000), the occurrence of igneous chondrule-like fragments suggest that it is also probable that they are pulverized dust of chondrules (Bridges et al., 2012). It is well-established that chondrules in different chondrite groups have different Mg#–Δ^{17}O trends (i) CV, CO, CM, and the ungrouped Acfer 094 chondrite chondrules are dominated by two populations, i.e., Mg# > 97 with Δ^{17}O ranges from –6‰ to –4‰ and Mg# ≤ 97 with Δ^{17}O ~ –2‰ (Ushikubo et al., 2012; Tenner et al., 2013; Chaumard et al., 2018; Hertwig et al., 2018); (ii) porphyritic chondrules in CH-CB chondrites have Δ^{17}O decreasing from +4‰ to –5‰ as their Mg# decreases from 99 to 96, and then varying irregularly between –2‰ to +3‰ when Mg# < 96 (Krot et al., 2010; Nakashima et al., 2019); and (iii) O and R, E and K chondrules have nearly zero or slightly positive Δ^{17}O values independent of their Mg# values (Kita et al., 2010; Weisberg et al., 2011; Nagashima et al., 2015; Miller et al., 2017); (iv) CR chondrite chondrules show a negative correlation between their Δ^{17}O and Mg#, that is, Δ^{17}O gradually increases from −6‰ to −1‰ as Mg# decreases from 99 to 94, and the rest, with Mg# < 90, show variable Δ^{17}O between –2‰ and +2‰ (Connolly and Huss, 2010; Schrader et al., 2013; Schrader et al., 2014; Tenner et al., 2015). The negative correlation between Mg# and Δ^{17}O was explained as adding ^{16}O-poor H_2O ice (Δ^{17}O > 0‰) to the reduced anhydrous dust (Δ^{17}O = −6‰) in the chondrule-forming region, which increases the dust/gas ratios and results in the formation of more oxidizing (lower Mg#) chondrules (Tenner et al., 2015). Obviously, the Mg#–Δ^{17}O trend in the giant cluster IDP is closest to the CR chondrite chondrules, where the K-S test returns a *p*-value of 0.051 (slightly higher than the commonly used threshold of 0.05) that supports they are possibly from the same population. The relatively low *p*-value is partly due to the higher abundance of iron-rich particles in the giant cluster IDP (11/20) than CR chondrite chondrules (~2 vol%) (Schrader et al., 2015), indicating that they formed in a more oxidizing environment with higher dust density. In contrast, the returned *p*-values for fragments in the giant cluster IDP and chondrules in other primitive chondrites are typically $<10^{-3}$, rejecting a genetic relationship between them.

4.3. Transportation of crystalline silicate fragments to the comet-forming region

As discussed above, crystalline silicate fragments in anhydrous IDPs (including the giant cluster IDP) are similar to those in Wild 2 particles on petrography, mineral chemistry, and oxygen isotope systematics, supporting a cometary origin of anhydrous IDPs. Among the 20 fragments in the giant cluster IDP, LT7, LT14, and possibly LT410 have an origin where O or R chondrite chondrules formed, fragment LT400 has affinities to R or CH-CB chondrules, and the remaining ones are closest to CR chondrite chondrules. Since *in situ* production of chondrules in the Kuiper belt region is unlikely (Nakamura et al., 2008), we believe that the giant cluster IDP accreted diverse materials formed in a wide solar system region like Wild 2 particles (Brownlee, 2014). However, the transportation mechanism of high-temperature materials into the comet-forming region remains unclear.

During the early expansion of an initially quite compact disk, turbulent diffusion can rapidly transport high-temperature inner-disk particles to the 25-30 AU comet-forming region, especially near the disk midplane (Ciesla, 2007). This model explains the presence of the oldest solid materials, CAIs and AOAs, in the comets. However, as the disk evolves, radial drift dominates over disk expansion, and therefore the outward velocity and flux decreases as more and more materials are lost onto the central star. While the presence of O chondrite chondrule-like fragments, which might have crystallized ~2 Ma after CAI formation (e.g., Siron et al., 2021), is consistent with a late accretion time (≥ 2.6 Ma after CAI formation) of comet Wild 2 (e.g., Ogliore et al., 2012; Nakashima et al., 2015), it is unknown whether turbulent diffusion can transport these late-formed fragments to the disk beyond 25 AU. Furthermore, the O/R chondrite chondrule-like fragment LT14, whose minerals are apparently in chemical disequilibrium, is thought to have undergone thermal metamorphism on the O/R-like parent body. The timing of the thermal metamorphism could have been as early as 2.5 Ma after CAI formation when the center of a ⩾100 km planetesimal was quickly raised above 800℃ before reaching maximum central temperatures of 850-950℃ at ~5 Ma (inferred peak metamorphic temperature for H6 and L6 chondrites) (Blackburn et al., 2017). Another important constraint is that the outward transportation of O chondrite chondrule-like fragments may be blocked by Jupiter's core, which is thought to grow up to ~20 M_E (M_E=the mass of the Earth) within 1 Ma (Kruijer et al., 2017). However, more and more O chondrite-like

chondrules and O chondrite-like relict olivine grains have been identified in carbonaceous chondrites by their distinct O, Cr, and Ti isotope signatures and mineral and chemical characteristics (e.g., Hertwig et al., 2018; Schrader et al., 2020; Williams et al., 2020). Thus, chondrule-sized or smaller fragments have nevertheless been transported from the O chondrite-forming region to the carbonaceous chondrite-forming regions ~2-3 Ma after CAI formation. Furthermore, these fragments may have been transferred farther to the comet-forming region if they were smashed in the inner disk (Bridges et al., 2012).

Hughes and Armitage (2010) presented a series of 1D models to explore the effects of particle size, disk evolution, and radial flow dynamics on the evolution of particles within a gas disk. They found that 20 μm particles (poorly-coupled with the gas motions) could not exist in the disk beyond 25 AU for >1 Ma under the accretion-flow dynamics. The O chondrite chondrule-like fragment LT7 with a size of 22 × 12 μm^2 found in the giant cluster IDP possibly suggests that this particle was retained in the disk beyond 25 AU for a relatively short period. Recently, Atacama Large Millimeter/submillimeter Array (ALMA) showed multiple well-defined and nearly perfectly circular rings in a large fraction of the protoplanetary disks, likely due to dust trapping in radial pressure bumps, indicating that the gas density does not always decrease with distance from the Sun (Dullemond et al., 2018). Thus, the coarse fragments could have been trapped in comparable circular rings for a certain period before comet accretion.

For the remaining CR-CH-CB chondrite chondrule-like fragments, the transportation distance is much shorter as parent bodies of these chondrites are considered to accrete at the disk beyond the orbits of the gas giants since they preserved significant amounts of thermally unprocessed, ^{26}Al-free primordial molecular cloud matters that may only survive in the outer part of the solar system (Van Kooten et al., 2016). Desch et al. (2018) constructed a protoplanetary disk based on the abundances of refractory elements and refractory inclusions in different chondrite groups and suggested that CR chondrites' parent body accreted ~4-5 Ma after CAI formation at 3.84-4 AU. At that time, most or all of the gas could have been lost via accretion onto the central star or dispersed via the photoevaporation process, and therefore particle transportation was likely limited. While more evidence is necessary to validate this hypothesis, it is reasonable to infer that the comets contain predominantly CR chondrite chondrule-like materials which formed and accreted nearby.

5. Conclusions

High precision (≤ 2‰ in $\Delta^{17}O$) oxygen isotope ratios of individual crystalline silicates in 20 fragments from a giant cluster IDP U2-20GCA were determined using a SIMS IMS-1280. The fragments are mainly monomineralic (6/20) or polymineralic (9/20) and composed of olivine and/or pyroxene, with the longest dimension ranging from 5 μm to 35 μm. Others are chondrule-like fragments including two BO-like, two PP-like, and one ARC-like. Unlike other anhydrous IDPs and Wild 2 particles showing Mg# distributions evenly from 100 to 58, the giant cluster IDP has an Mg# distribution bimodally at > 90 and 75-80. Fe vs. Mn abundances in olivine of anhydrous IDPs are uncorrelated and span a wide range similar to Wild 2 particles and CR chondrite chondrules. Low chromium concentrations (≤0.1 wt% Cr_2O_3) in the giant cluster IDP's iron-rich olivines may suggest that they underwent mild thermal metamorphism like Wild 2 particles. The fragments are ^{16}O-poor with $\delta^{18}O$ and $\delta^{17}O$ varying from –6.2 ± 1.0‰ to 6.8 ± 1.9‰ and–6.7 ± 2.6‰ to 5.3 ± 1.2‰, respectively. This range is similar to the CR chondrite chondrules but narrower than the Wild 2 ^{16}O-poor particles. $\Delta^{17}O$ are systematically lower for fragments with higher Mg# (> 90) than those with lower Mg# (70-80), showing a similar trend to Wild 2 particles and CR chondrite chondrules. These similarities demonstrate a cometary origin of anhydrous IDPs, and CR chondrite chondrule-like materials are likely the main source of crystalline silicates in the parent comets of anhydrous IDPs.

As exceptions, three fragments have resolvable positive $\delta^{18}O$, $\delta^{17}O$ values that overlap with O-R chondrite chondrules (LT7 and LT14) and CH-CB chondrite chondrules (LT400), suggesting origins similar to O, R, or CH-CB chondrite chondrules, respectively. LT14, composed of iron-rich olivine and magnesium-rich pyroxene, likely experienced thermal metamorphism on the O/R chondrite parent body. $\Delta^{17}O$ of the ARC-like fragment LT410 (–1.4 ± 1.4‰) falls in the range of ARCs in O and CR-CH chondrites. The presence of O chodnrite chondrule-like fragments in the giant cluster IDP, which likely crystallized 2-3 Ma after CAI formation, suggests that inner solar system materials were transported into the comet-forming region independent of Jupiter's existence.

Acknowledgments

The authors thank Bil Schneider for assistance with SEM imaging and Michael Spicuzza for technical assistance with SIMS operation. We are grateful to two anonymous reviewers for helpful comments and Frédéric Moynier for editor handling. This work is supported by the NASA programs (NNX16AG80G, N.K.). The WiscSIMS laboratory is partly supported by NSF (NNX17AE29G). Support for FIB instrumentation was provided by the University of Wisconsin-Madison Office of the Vice-Chancellor for Research and Graduate Education with funding from the Wisconsin Alumni Research Foundation, the College of Engineering, and the NSF Materials Research and Engineering Center (NSF DMR-1121288).

References

Aléon, J., Engrand, C., Leshin, L.A., McKeegan, K.D., 2009. Oxygen isotopic composition of chondritic interplanetary dust particles: A genetic link between carbonaceous chondrites and comets. Geochim. Cosmochim. Acta 73, 4558-4575. http://dx.doi.org/10.1016/j.gca.2009.04.034.

Berlin, J., Jones, R.H., Brearley, A.J., 2011. Fe-Mn systematics of type IIA chondrules in unequilibrated CO, CR, and ordinary chondrites. Meteorit. Planet. Sci 46, 513-533. https://doi.org/10.1111/j.1945-5100.2011.01171.x.

Blackburn, T., Alexander, C.M.O.D., Carlson, R., Elkins-Tanton, L.T., 2017. The accretion and impact history of the ordinary chondrite parent bodies. Geochim. Cosmochim. Acta 200, 201-217. https://doi.org/10.1016/j.gca.2016.11.038.

Bradley, J.P., 2014. 1.8 - Early solar nebula grains-Interplanetary dust particles, in: Holland, H.D., Turekian, K.K. (Eds.), Treatise on Geochemistry (Second Edition). Elsevier, Oxford, pp. 287-308.

Brearley, A.J., Jones, R.H., 1998. Chondritic meteorites, in: Papike, J.J. (Ed.), Planetary Materials. Mineralogical Society of America, Washington, D.C, pp. 31-398.

Bridges, J.C., Changela, H.G., Nayakshin, S., Starkey, N.A., Franchi, I.A., 2012. Chondrule fragments from Comet Wild2: Evidence for high temperature processing in the outer Solar System. Earth planet. Sci Lett. 341-344, 186-194. https://doi.org/10.1016/j.epsl.2012.06.011.

Brownlee, D.E., 2014. The Stardust Mission: Analyzing Samples from the Edge of the Solar System. Annu. Rev. Earth Planet. Sci. 42, 179-205. https://doi.org/10.1146/annurev-earth-050212-124203.

Brownlee, D.E., Joswiak, D.J., 2017. Diversity of the initial rocky planetary building materials at the edge of the solar system. Meteorit. Planet. Sci 52, 471-478. https://doi.org/10.1111/maps.12804.

Busemann, H., Nguyen, A.N., Cody, G.D., Hoppe, P., Kilcoyne, A.L.D., Stroud, R.M., Zega, T.J., Nittler, L.R., 2009. Ultra-primitive interplanetary dust particles from the comet 26P/Grigg–Skjellerup dust stream collection. Earth planet. Sci Lett. 288, 44-57. https://doi.org/10.1016/j.epsl.2009.09.007.

Chaumard, N., Defouilloy, C., Kita, N.T., 2018. Oxygen isotope systematics of chondrules in the Murchison CM2 chondrite and implications for the CO-CM relationship. Geochim. Cosmochim. Acta 228, 220-242. https://doi.org/10.1016/j.gca.2018.02.040.

Ciesla, F.J., 2007. Outward transport of high-temperature materials around the midplane of the solar nebula. Science 318, 613-615. https://doi.org/10.1126/science.1147273.

444 Clayton, R.N., Grossman, L., Mayeda, T.K., 1973. A component of primitive nuclear composition in
445 carbonaceous meteorites. Science 182, 485-488. https://doi.org/10.1126/science.182.4111.485.

446 Connolly, J.H.C., Huss, G.R., 2010. Compositional evolution of the protoplanetary disk: Oxygen isotopes of
447 type-II chondrules from CR2 chondrites. Geochim. Cosmochim. Acta 74, 2473-2483.
448 http://dx.doi.org/10.1016/j.gca.2010.01.005.

449 Davidson, J., Alexander, C.M.O.D., Stroud, R.M., Busemann, H., Nittler, L.R., 2019. Mineralogy and
450 petrology of Dominion Range 08006: A very primitive CO3 carbonaceous chondrite. Geochim.
451 Cosmochim. Acta. https://doi.org/10.1016/j.gca.2019.08.032.

452 Defouilloy, C., Nakashima, D., Joswiak, D.J., Brownlee, D.E., Tenner, T.J., Kita, N.T., 2017. Origin of
453 crystalline silicates from Comet 81P/Wild 2: Combined study on their oxygen isotopes and mineral
454 chemistry. Earth planet. Sci Lett. 465, 145-154. https://doi.org/10.1016/j.epsl.2017.02.045.

455 Desch, S.J., Kalyaan, A., Alexander, C.M.O.D., 2018. The effect of Jupiter's formation on the distribution of
456 refractory elements and inclusions in meteorites. Astrophys. J. Suppl. Ser. 238, 11.
457 https://doi.org/10.3847/1538-4365/aad95f.

458 Dullemond, C.P., Birnstiel, T., Huang, J., Kurtovic, N.T., Andrews, S.M., Guzmán, V.V., Pérez, L.M., Isella,
459 A., Zhu, Z., Benisty, M.J.T.A.J.L., 2018. The disk substructures at high angular resolution project
460 (DSHARP). VI. Dust trapping in thin-ringed protoplanetary disks. Astrophys. J. 869, L46.
461 https://doi.org/10.3847/2041-8213/aaf742.

462 Frank, D.R., Zolensky, M.E., Le, L., 2014. Olivine in terminal particles of Stardust aerogel tracks and
463 analogous grains in chondrite matrix. Geochim. Cosmochim. Acta 142, 240-259.
464 https://doi.org/10.1016/j.gca.2014.05.037.

465 Gainsforth, Z., Butterworth, A.L., Stodolna, J., Westphal, A.J., Huss, G.R., Nagashima, K., Ogliore, R.,
466 Brownlee, D.E., Joswiak, D., Tyliszczak, T., Simionovici, A.S., 2015. Constraints on the formation
467 environment of two chondrule-like igneous particles from comet 81P/Wild 2. Meteorit. Planet. Sci 50,
468 976-1004. https://doi.org/10.1111/maps.12445.

469 Ganguly, J., Tazzoli, V., 1994. Fe^{2+}-Mg interdiffusion in orthopyroxene: Retrieval from the data on
470 intracrystalline exchange reaction. Am. Mineral 79, 930-937.

471 Hertwig, A.T., Defouilloy, C., Kita, N.T., 2018. Formation of chondrules in a moderately high dust enriched
472 disk: evidence from oxygen isotopes of chondrules from the Kaba CV3 chondrite. Geochim. Cosmochim.
473 Acta 224, 116-131. https://doi.org/10.1016/j.gca.2017.12.013.

474 Hicks, L.J., MacArthur, J.L., Bridges, J.C., Price, M.C., Wickham-Eade, J.E., Burchell, M.J., Hansford, G.M.,
475 Butterworth, A.L., Gurman, S.J., Baker, S.H., 2017. Magnetite in Comet Wild 2: Evidence for parent
476 body aqueous alteration. Meteorit. Planet. Sci 52, 2075-2096. https://doi.org/10.1111/maps.12909.

477 Hughes, A.L., Armitage, P.J., 2010. Particle transport in evolving protoplanetary disks: implications for results
478 from Stardust. Astrophys. J. 719, 1633. https://doi.org/10.1088/0004-637X/719/2/1633.

479 Ishii, H.A., Bradley, J.P., Dai, Z.R., Chi, M., Kearsley, A.T., Burchell, M.J., Browning, N.D., Molster, F.,
480 2008. Comparison of comet 81P/Wild 2 dust with interplanetary dust from comets. Science 319, 447-450.
481 https://doi.org/10.1126/science.1150683.

482 Joswiak, D.J., Brownlee, D.E., Matrajt, G., Westphal, A.J., Snead, C.J., 2009. Kosmochloric Ca-rich
483 pyroxenes and FeO-rich olivines (Kool grains) and associated phases in Stardust tracks and chondritic
484 porous interplanetary dust particles: Possible precursors to FeO-rich type II chondrules in ordinary
485 chondrites. Meteorit. Planet. Sci 44, 1561-1588. https://doi.org/10.1111/j.1945-5100.2009.tb01192.x.

486 Joswiak, D.J., Brownlee, D.E., Matrajt, G., Westphal, A.J., Snead, C.J., Gainsforth, Z., 2012. Comprehensive
487 examination of large mineral and rock fragments in Stardust tracks: Mineralogy, analogous
488 extraterrestrial materials, and source regions. Meteorit. Planet. Sci 47, 471-524.
489 https://doi.org/10.1111/j.1945-5100.2012.01337.x.

Joswiak, D.J., Nakashima, D., Brownlee, D.E., Matrajt, G., Ushikubo, T., Kita, N.T., Messenger, S., Ito, M., 2014. Terminal particle from Stardust track 130: Probable Al-rich chondrule fragment from comet Wild 2. Geochim. Cosmochim. Acta 144, 277-298. https://doi.org/10.1016/j.gca.2014.08.017.

Joswiak, D.J., Brownlee, D.E., Nguyen, A.N., Messenger, S., 2017. Refractory materials in comet samples. Meteorit. Planet. Sci 52, 1612-1648. https://doi.org/10.1111/maps.12877.

Kita, N.T., Nagahara, H., Tachibana, S., Tomomura, S., Spicuzza, M.J., Fournelle, J.H., Valley, J.W., 2010. High precision SIMS oxygen three isotope study of chondrules in LL3 chondrites: Role of ambient gas during chondrule formation. Geochim. Cosmochim. Acta 74, 6610-6635. http://dx.doi.org/10.1016/j.gca.2010.08.011.

Krot, A.N., Nagashima, K., Yoshitake, M., Yurimoto, H., 2010. Oxygen isotopic compositions of chondrules from the metal-rich chondrites Isheyevo (CH/CBb), MAC 02675 (CBb) and QUE 94627 (CBb). Geochim. Cosmochim. Acta 74, 2190-2211. http://dx.doi.org/10.1016/j.gca.2009.12.013.

Krot, A.N., Nagashima, K., van Kooten, E.M.M., Bizzarro, M., 2017. Calcium–aluminum-rich inclusions recycled during formation of porphyritic chondrules from CH carbonaceous chondrites. Geochim. Cosmochim. Acta 201, 185-223. http://dx.doi.org/10.1016/j.gca.2016.09.001.

Kruijer, T.S., Burkhardt, C., Budde, G., Kleine, T., 2017. Age of Jupiter inferred from the distinct genetics and formation times of meteorites. Proceedings of the National Academy of Sciences 114, 6712-6716. https://www.pnas.org/content/114/26/6712.short.

Matrajt, G., Messenger, S., Brownlee, D., Joswiak, D., 2012. Diverse forms of primordial organic matter identified in interplanetary dust particles. Meteorit. Planet. Sci 47, 525-549. https://doi.org/10.1111/j.1945-5100.2011.01310.x.

McKeegan, K.D., Aléon, J., Bradley, J., Brownlee, D., Busemann, H., Butterworth, A., Chaussidon, M., Fallon, S., Floss, C., Gilmour, J., 2006. Isotopic compositions of cometary matter returned by Stardust. Science 314, 1724-1728. http://dx.doi.org/10.1126/science.1135992.

Miller, K.E., Lauretta, D.S., Connolly, H.C., Berger, E.L., Nagashima, K., Domanik, K., 2017. Formation of unequilibrated R chondrite chondrules and opaque phases. Geochim. Cosmochim. Acta 209, 24-50. https://doi.org/10.1016/j.gca.2017.04.009.

Nagashima, K., Krot, A.N., Huss, G.R., 2015. Oxygen-isotope compositions of chondrule phenocrysts and matrix grains in Kakangari K-grouplet chondrite: Implication to a chondrule-matrix genetic relationship. Geochim. Cosmochim. Acta 151, 49-67. https://doi.org/10.1016/j.gca.2014.12.012.

Nakamura, T., Noguchi, T., Tsuchiyama, A., Ushikubo, T., Kita, N.T., Valley, J.W., Zolensky, M.E., Kakazu, Y., Sakamoto, K., Mashio, E., Uesugi, K., Nakano, T., 2008. Chondrulelike objects in short-period comet 81P/Wild 2. Science 321, 1664-1667. http://dx.doi.org/10.1126/science.1160995.

Nakashima, D., Ushikubo, T., Joswiak, D.J., Brownlee, D.E., Matrajt, G., Weisberg, M.K., Zolensky, M.E., Kita, N.T., 2012a. Oxygen isotopes in crystalline silicates of comet Wild 2: A comparison of oxygen isotope systematics between Wild 2 particles and chondritic materials. Earth planet. Sci Lett. 357-358, 355-365. https://doi.org/10.1016/j.epsl.2012.09.041.

Nakashima, D., Ushikubo, T., Zolensky, M.E., Kita, N.T., 2012b. High precision oxygen three-isotope analyses of anhydrous chondritic interplanetary dust particles. Meteorit. Planet. Sci 47, 197-208. http://dx.doi.org/10.1111/j.1945-5100.2011.01319.x.

Nakashima, D., Ushikubo, T., Kita, N.T., Weisberg, M.K., Zolensky, M.E., Ebel, D.S., 2015. Late formation of a comet Wild 2 crystalline silicate particle, Pyxie, inferred from Al–Mg chronology of plagioclase. Earth planet. Sci Lett. 410, 54-61. https://doi.org/10.1016/j.epsl.2014.11.020.

Nakashima, D., Kimura, M., Yamada, K., Noguchi, T., Ushikubo, T., Kita, N.T., 2019. Oyxgen isotope systematics of porphyritic chondrules and their fragments in CH and CB chondrites. In: 82nd Annual Meeting of The Meteoritical Society. (Abstr.#6043).

536 Nittler, L.R., Stroud, R.M., Trigo-Rodríguez, J.M., De Gregorio, B.T., Alexander, C.M.O.D., Davidson, J.,
537 Moyano-Cambero, C.E., Tanbakouei, S., 2019. A cometary building block in a primitive asteroidal
538 meteorite. Nat. Astron. 3, 659-666. https://doi.org/10.1038/s41550-019-0737-8.

539 Nuth, J.A., Hill, H.G.M., Kletetschka, G., 2000. Determining the ages of comets from the fraction of
540 crystalline dust. Nature 406, 275-276. http://dx.doi.org/10.1038/35018516.

541 Ogliore, R.C., Huss, G.R., Nagashima, K., Butterworth, A.L., Gainsforth, Z., Stodolna, J., Westphal, A.J.,
542 Joswiak, D., Tyliszczak, T., 2012. Incorporation of a late-forming chondrule into comet Wild 2.
543 Astrophys. J. 745, L19. http://dx.doi.org/10.1088/2041-8205/745/2/L19.

544 Ogliore, R.C., Nagashima, K., Huss, G.R., Westphal, A.J., Gainsforth, Z., Butterworth, A.L., 2015. Oxygen
545 isotopic composition of coarse- and fine-grained material from comet 81P/Wild 2. Geochim. Cosmochim.
546 Acta 166, 74-91. https://doi.org/10.1016/j.gca.2015.04.028.

547 Sandford, S.A., Bradley, J.P., 1989. Interplanetary dust particles collected in the stratosphere: Observations of
548 atmospheric heating and constraints on their interrelationship and sources. Icarus 82, 146-166.
549 https://doi.org/10.1016/0019-1035(89)90028-6.

550 Schrader, D.L., Connolly, H.C., Lauretta, D.S., Nagashima, K., Huss, G.R., Davidson, J., Domanik, K.J., 2013.
551 The formation and alteration of the Renazzo-like carbonaceous chondrites II: Linking O-isotope
552 composition and oxidation state of chondrule olivine. Geochim. Cosmochim. Acta 101, 302-327.
553 https://doi.org/10.1016/j.gca.2012.09.045.

554 Schrader, D.L., Nagashima, K., Krot, A.N., Ogliore, R.C., Hellebrand, E., 2014. Variations in the O-isotope
555 composition of gas during the formation of chondrules from the CR chondrites. Geochim. Cosmochim.
556 Acta 132, 50-74. https://doi.org/10.1016/j.gca.2014.01.034.

557 Schrader, D.L., Connolly Jr., H.C., Lauretta, D.S., Zega, T.J., Davidson, J., Domanik, K.J., 2015. The
558 formation and alteration of the Renazzo-like carbonaceous chondrites III: Toward understanding the
559 genesis of ferromagnesian chondrules. Meteorit. Planet. Sci 50, 15-50.
560 https://doi.org/10.1111/maps.12402.

561 Schrader, D.L., Nagashima, K., Davidson, J., McCoy, T.J., Ogliore, R.C., Fu, R.R., 2020. Outward migration
562 of chondrule fragments in the Early Solar System: O-isotopic evidence for rocky material crossing the
563 Jupiter Gap? Geochim. Cosmochim. Acta. https://doi.org/10.1016/j.gca.2020.05.014.

564 Siron, G., Fukuda, K., Kimura, M., Kita, N.T., 2021. New constraints from ^{26}Al-^{26}Mg chronology of anorthite
565 bearing chondrules in unequilibrated ordinary chondrites. Geochim. Cosmochim. Acta 293, 103-126.
566 https://doi.org/10.1016/j.gca.2020.10.025.

567 Starkey, N.A., Franchi, I.A., Lee, M.R., 2014. Isotopic diversity in interplanetary dust particles and
568 preservation of extreme ^{16}O-depletion. Geochim. Cosmochim. Acta 142, 115-131.
569 https://doi.org/10.1016/j.gca.2014.07.011.

570 Stodolna, J., Jacob, D., Leroux, H., 2012. Mineralogy and petrology of Stardust particles encased in the bulb of
571 track 80: TEM investigation of the Wild 2 fine-grained material. Geochim. Cosmochim. Acta 87, 35-50.
572 https://doi.org/10.1016/j.gca.2012.03.026.

573 Tenner, T.J., Ushikubo, T., Kurahashi, E., Kita, N.T., Nagahara, H., 2013. Oxygen isotope systematics of
574 chondrule phenocrysts from the CO3.0 chondrite Yamato 81020: Evidence for two distinct oxygen
575 isotope reservoirs. Geochim. Cosmochim. Acta 102, 226-245.
576 http://dx.doi.org/10.1016/j.gca.2012.10.034.

577 Tenner, T.J., Nakashima, D., Ushikubo, T., Kita, N.T., Weisberg, M.K., 2015. Oxygen isotope ratios of FeO-
578 poor chondrules in CR3 chondrites: Influence of dust enrichment and H_2O during chondrule formation.
579 Geochim. Cosmochim. Acta 148, 228-250. http://dx.doi.org/10.1016/j.gca.2014.09.025.

Ushikubo, T., Kimura, M., Kita, N.T., Valley, J.W., 2012. Primordial oxygen isotope reservoirs of the solar nebula recorded in chondrules in Acfer 094 carbonaceous chondrite. Geochim. Cosmochim. Acta 90, 242-264. http://dx.doi.org/10.1016/j.gca.2012.05.010.

Van Kooten, E.M., Wielandt, D., Schiller, M., Nagashima, K., Thomen, A., Larsen, K.K., Olsen, M.B., Nordlund, Å., Krot, A.N., Bizzarro, M., 2016. Isotopic evidence for primordial molecular cloud material in metal-rich carbonaceous chondrites. Proceedings of the National Academy of Sciences 113, 2011-2016. https://doi.org/10.1073/pnas.1518183113.

Weisberg, M.K., Ebel, D.S., Connolly, H.C., Kita, N.T., Ushikubo, T., 2011. Petrology and oxygen isotope compositions of chondrules in E3 chondrites. Geochim. Cosmochim. Acta 75, 6556-6569. https://doi.org/10.1016/j.gca.2011.08.040.

Williams, C.D., Sanborn, M.E., Defouilloy, C., Yin, Q.-Z., Kita, N.T., Ebel, D.S., Yamakawa, A., Yamashita, K., 2020. Chondrules reveal large-scale outward transport of inner Solar System materials in the protoplanetary disk. Proceedings of the National Academy of Sciences, 202005235. https://doi.org/10.1073/pnas.2005235117.

Young, E.D., Russell, S.S., 1998. Oxygen reservoirs in the early solar nebula inferred from an Allende CAI. Science 282, 452-455. https://doi.org/10.1126/science.282.5388.452.

Zhang, M., Lin, Y., Tang, G., Liu, Y., Leya, I., 2020. Origin of Al-rich chondrules in CV chondrites: Incorporation of diverse refractory components into the ferromagnesian chondrule-forming region. Geochim. Cosmochim. Acta 272, 198-217. https://doi.org/10.1016/j.gca.2019.12.011.

Zolensky, M.E., Zega, T.J., Yano, H., Wirick, S., Westphal, A.J., Weisberg, M.K., Weber, I., Warren, J.L., Velbel, M.A., Tsuchiyama, A., Tsou, P., Toppani, A., Tomioka, N., Tomeoka, K., Teslich, N., Taheri, M., Susini, J., Stroud, R., Stephan, T., Stadermann, F.J., Snead, C.J., Simon, S.B., Simionovici, A., See, T.H., Robert, F., Rietmeijer, F.J.M., Rao, W., Perronnet, M.C., Papanastassiou, D.A., Okudaira, K., Ohsumi, K., Ohnishi, I., Nakamura-Messenger, K., Nakamura, T., Mostefaoui, S., Mikouchi, T., Meibom, A., Matrajt, G., Marcus, M.A., Leroux, H., Lemelle, L., Le, L., Lanzirotti, A., Langenhorst, F., Krot, A.N., Keller, L.P., Kearsley, A.T., Joswiak, D., Jacob, D., Ishii, H., Harvey, R., Hagiya, K., Grossman, L., Grossman, J.N., Graham, G.A., Gounelle, M., Gillet, P., Genge, M.J., Flynn, G., Ferroir, T., Fallon, S., Ebel, D.S., Dai, Z.R., Cordier, P., Clark, B., Chi, M., Butterworth, A.L., Brownlee, D.E., Bridges, J.C., Brennan, S., Brearley, A., Bradley, J.P., Bleuet, P., Bland, P.A., Bastien, R., 2006. Mineralogy and petrology of comet 81P/Wild 2 nucleus samples. Science 314, 1735-1739. https://doi.org/10.1126/science.1135842.

Figure Captions

Fig. 1. BSE (a-c, e-g) and TEM bright-field (d, h) images of eight representative crystalline silicate fragments in the giant cluster IDP. *Abbreviation*: Sul = sulfide; Ka = kamacite; Sch = schreibersite; Mt = magnetite (formed during atmospheric entry); Po = pyrrhotite; Gl = feldspathic glass; Chr = chromite; Al-Di = Al-diopside; An = anorthite; Pl = plagioclase; others used as previous. Scale bars are 5 μm. [Color is not needed in print]

Fig. 2. Mean oxygen isotope ratios of crystalline silicate fragments in the giant cluster IDP. Data of crystalline silicate fragments in Wild 2 particles (Nakamura et al., 2008; Nakashima et al., 2012a; Joswiak et al., 2014; Ogliore et al., 2015; Defouilloy et al., 2017) and other anhydrous IDPs (Aléon et al., 2009; Nakashima et al., 2012b) are shown for comparison. Black arrows indicate Chondrule-like fragments and the three mono/polymineralic fragments (Lt4, LT14, and LT400) with positive oxygen isotope ratios that plot above the terrestrial fractionation (TF) line. *Abbreviation*: CCAM = carbonaceous chondrite anhydrous mineral line (Clayton et al., 1973); Y&R = Young & Russell line (Young and Russell, 1998); PCM = primitive chondrule minerals line (Ushikubo et al., 2012). [Color is not needed in print]

Fig.3. Fe vs. Mn (afu = atomic formula units based on four oxygen atoms) of olivine in crystalline silicate fragments of the giant cluster IDP. Data of other anhydrous IDPs (Brownlee and Joswiak, 2017), Wild 2 particles (Joswiak et al., 2012; Frank et al., 2014; Brownlee and Joswiak, 2017), and CR chondrite chondrules (Schrader et al., 2015) are shown for comparison. LT14 with elevated MnO content plots close to the line defined by O chondrite (OC), while other iron-rich olivines plot between the two lines defined by O and CO chondrites (Berlin et al., 2011). [Color is not needed in print]

Fig.4. Fa [atom% Fe/(Fe+Mg)] vs. Cr_2O_3 of olivine in crystalline silicate fragments of the giant cluster IDP. Data of Wild 2 particles and O chondrites (L/LL3.0-3.1 and LL3.2) [(Frank et al., 2014) and references therein], CO3.0-3.1 (Davidson et al., 2019), and CR (Schrader et al., 2015) chondrites are plotted for comparison. The iron-rich olivines are depleted in Cr_2O_3 like Wild 2 particles, possibly suggesting mild thermal metamorphism. [Color is not needed in print]

Fig.5. Mean oxygen isotope ratios of crystalline silicate fragments in the giant cluster IDP as compared with chondrules in CR (Connolly and Huss, 2010; Schrader et al., 2013; Schrader et al., 2014; Tenner et al., 2015), CH-CB (Krot et al., 2010), CV (Hertwig et al., 2018), CO (Tenner et al., 2013), CM (Chaumard et al., 2018), the ungrouped Acfer 094 (Ushikubo et al., 2012), O (Kita et al., 2010), R (Miller et al., 2017), K (Nagashima et al., 2015), and E chondrites (Weisberg et al., 2011). In O-R and E-K groups, chondrules have nearly identical oxygen isotope ranges and plots in the same legends for simplicity. [Color is not needed in print]

643 Fig. 6. Mg# vs. $\Delta^{17}O$ of crystalline silicate fragments in the giant cluster IDP (a) compared with Wild 2
644 particles (b) and primitive chondrite chondrules (c, d). Data are from references listed in the caption of Fig. 5.
645 In panel (a), literature data (Aléon et al., 2009), and fragments that likely have O-R or CH-CB origins and
646 other fragments in the giant cluster IDP, are shown in different legends. [Color is not needed in print]

647

Table 1. EDX major elements of crystalline silicate fragments in the giant cluster IDP

Fragment	Size	Petrography	Target	SiO_2	MgO	FeO	CaO	Al_2O_3	Cr_2O_3	MnO	TiO_2	Na_2O	Fo/En	Wo
LT2	22 × 18	Polymineral	Ol	38.3	40.8	19.8	0.18	0.47	0.12	0.40	---	---	78.8	
			Pig	55.5	24.9	11.0	3.66	4.08	0.56	0.29	---	---	74.0	7.78
LT4	35 × 10	Monomineral	En	60.7	33.9	3.30	0.40	0.15	0.84	0.52	---	0.25	94.1	0.79
LT5	15 × 25	Polymineral	En	57.8	32.4	4.52	1.47	1.29	1.18	1.33	---	---	90.1	2.92
LT6	15 × 10	Polymineral	Ol	37.9	39.2	22.5	0.15	---	---	0.23	---	---	75.8	
			Pig	53.0	26.8	15.8	2.12	1.82	0.24	0.27	---	---	72.2	4.08
LT7	22 × 12	Polymineral	Ol	37.4	40.8	21.4	0.14	---	---	0.21	---	---	77.4	
			Pig	54.6	27.1	13.0	2.53	1.92	0.61	0.24	---	---	75.0	5.00
LT9	11 × 4	Monomineral	Pig	52.5	25.5	11.2	4.39	5.17	0.28	0.45	0.55	---	73.1	9.00
LT11	12 × 6	Chondrule-Frag	En	57.9	34.9	1.56	1.64	2.15	1.14	0.40	0.36	---	94.5	3.17
LT13	10 × 6	Monomineral	Ol	39.3	39.4	20.8	0.22	---	---	0.30	---	---	77.4	
LT14	5 × 5	Polymineral	Ol	38.0	40.9	20.5	---	---	0.10	0.54	---	---	78.2	
			En	57.6	38.7	2.53	---	---	1.07	0.15	---	---	96.5	0.00
LT16	15 × 12	Polymineral	Ol	37.5	41.0	21.2	---	---	---	0.25	---	---	77.7	
			Pig	54.1	27.3	12.4	2.84	3.10	---	0.33	---	---	75.3	5.60
LT17	7 × 6	BO chondrule	Ol + Mes	39.9	46.2	13.4	---	---	---	0.50	---	---	86.1	
LT18	7 × 5	Monomineral	En	58.4	37.6	0.81	0.61	0.99	0.89	0.31	0.36	---	97.7	1.13
LT19	13 × 7	Monomineral	Ol	37.5	40.6	21.3	---	0.28	---	0.25	---	---	77.4	
LT20	15 × 4	Polymineral	Aug	52.8	26.8	5.89	9.04	3.04	0.99	0.46	0.77	0.15	73.4	17.66
LT23	11 × 8	BO chondrule	Ol + Mes	40.1	36.6	21.5	0.49	---	0.38	0.94	---	---	75.3	
LT24	28 × 14	Chondrule-Frag	En	61.9	31.1	3.85	0.87	0.92	0.90	0.36	0.10	---	91.9	1.83
LT26	11 × 7	Polymineral	Ol	38.4	39.8	20.7	0.88	---	---	0.20	---	---	77.6	
			Pig	54.8	26.2	13.5	2.71	1.89	0.56	0.29	---	---	73.5	5.43
LT35	15 × 25	Polymineral	Ol	43.1	54.9	0.78	0.24	---	0.74	0.18	---	---	99.2	
LT400	5 × 3	Monomineral	Ol	39.2	39.2	20.8	0.26	0.29	---	0.26	---	---	77.2	
LT410	9 × 5	ARC-like	Ol	42.5	55.8	0.84	0.16	---	0.67	0.11	---	---	99.2	

Fo = mol% Mg/(Mg+Fe); En = mol% Mg/(Mg+Fe+Ca); Wo = mol% Ca/(Mg+Fe+Ca). *Abbreviations*: Chondrule-Frag = chondrule fragment; BO = barred-olivine; Ol = olivine; Pig = pigeonite; En = enstatite; Mes = mesostasis; Aug = augite; ARC = Al-rich chondrule.

Table. 2 Mean oxygen isotope ratios of crystalline silicate fragments in the giant cluster IDP

IDPs	Mineral	Mg#	N	$\delta^{18}O$	2σ	$\delta^{17}O$	2σ	$\Delta^{17}O$	2σ
LT2	Ol	78.8	4	3.97	1.32	1.86	1.77	-0.20	1.61
	Pig	80.2	5	5.67	1.13	3.24	1.27	0.29	0.98
	Average	*79.5*	*9*	*4.91*	*1.11*	*2.63*	*1.18*	*0.07*	*0.93*
LT4	En	94.9	5	-1.30	1.02	-3.78	2.17	-3.10	2.43
LT5	En	92.8	5	-2.86	1.56	-1.83	1.60	-0.35	1.73
LT6	Ol	75.8	3	5.06	1.84	3.98	1.28	1.36	1.37
	Pig	72.3	1	4.50	2.61	3.06	1.86	0.72	2.02
	Average	*74.0*	*4*	*4.92*	*1.68*	*3.75*	*1.17*	*1.20*	*1.24*
LT7	Ol	77.4	1	0.69	1.08	1.08	2.36	0.72	2.02
	Pig	75.0	3	-1.22	2.61	0.31	1.69	0.94	1.97
	Average	*76.2*	*4*	*-0.74*	*2.11*	*0.50*	*1.54*	*0.88*	*1.51*
LT9	Pig	80.3	1	0.09	1.74	-1.61	3.08	-1.66	2.68
LT11	En	97.6	1	1.11	1.60	-0.31	1.37	-0.89	1.76
LT13	Ol	77.4	4	3.12	1.15	1.52	0.87	-0.10	0.97
LT14	Ol	78.2	1	-0.06	0.56	0.35	1.63	0.38	1.41
	En	96.0	1	0.64	0.56	2.21	1.63	1.88	1.41
	Average		*2*	*0.29*	*0.89*	*1.28*	*1.99*	*1.13*	*1.60*
LT16	Ol	77.7	2	2.74	1.49	0.67	1.70	-0.75	2.15
	Pig	75.4	2	1.06	1.49	0.08	1.67	-0.47	1.05
	Average	*76.6*	*4*	*1.90*	*1.40*	*0.38*	*1.33*	*-0.61*	*1.07*
LT17	Ol + Mes	86.2	3	-0.14	1.17	-2.43	1.36	-2.36	1.59
LT18	En	98.8	4	-0.10	1.20	-2.86	1.17	-2.81	1.35
LT19	Ol	77.4	2	0.09	1.74	-1.61	3.08	-1.66	2.68
LT20	Aug	89.1	2	-1.85	1.51	-3.74	2.04	-2.78	1.84
LT23	Ol + Mes	75.3	5	1.65	1.12	0.05	0.81	-0.81	1.03
LT24	En	93.6	4	1.09	0.69	-1.70	1.34	-2.27	1.35
LT26	Ol	77.6	2	3.17	1.28	2.34	1.87	0.69	1.56
	Pig	77.8	1	1.47	1.44	-0.12	2.27	-0.89	1.72
	Average	*77.7*	*3*	*2.60*	*1.39*	*1.52*	*2.11*	*0.17*	*1.50*
LT35	Ol	99.2	2	-6.09	0.93	-6.36	2.08	-3.20	2.00
LT400	Ol	77.2	1	3.35	0.93	5.16	1.35	3.42	1.63
LT410	Ol	99.2	4	-1.82	1.30	-2.29	1.65	-1.35	1.44

650

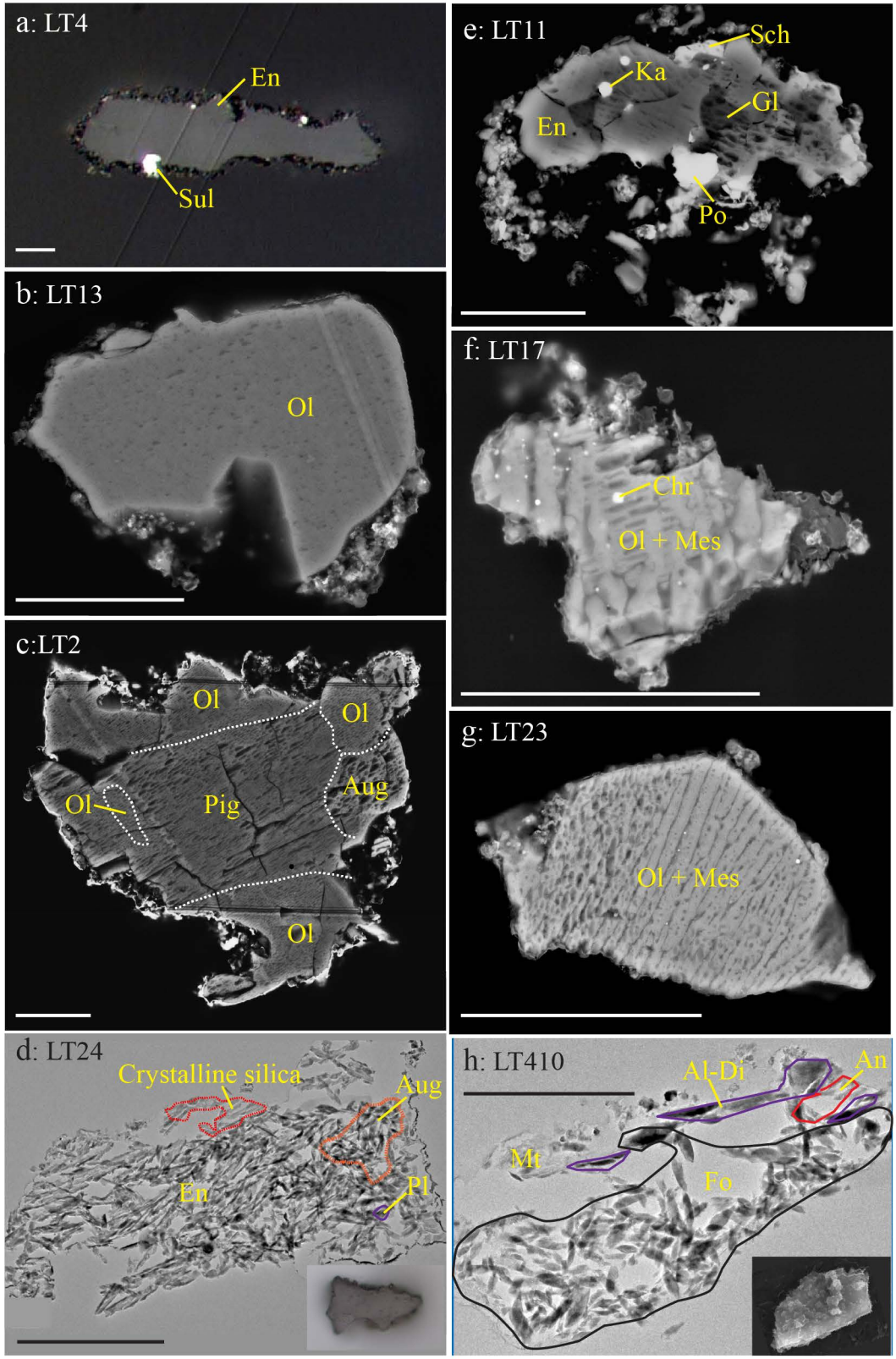
a: LT4
En
Sul
b: LT13
Ol
c:LT2
Ol
Ol
Ol
Pig
Aug
Ol
d: LT24
Crystalline silica
Aug
En
Pl
e: LT11
Sch
Ka
Gl
En
Po
f: LT17
Chr
Ol + Mes
g: LT23
Ol + Mes
h: LT410
Al-Di
An
Mt
Fo

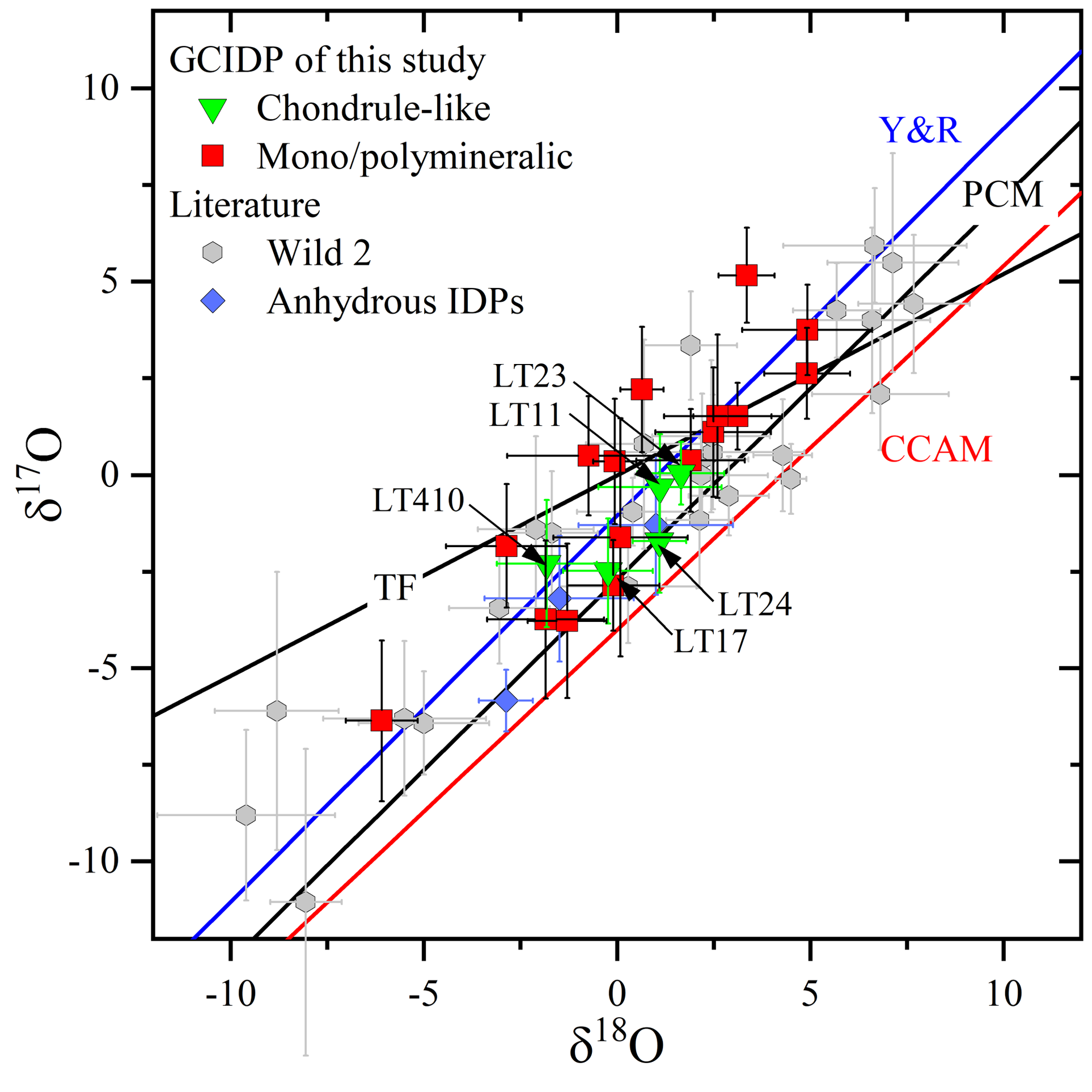
GCIDP of this study
Chondrule-like
Mono/polymineralic
Literature
Wild 2
Anhydrous IDPs
Y&R
PCM
CCAM
LT23
LT11
LT410
TF
LT24
LT17
10
5
0
-5
-10
δ17O
δ18O

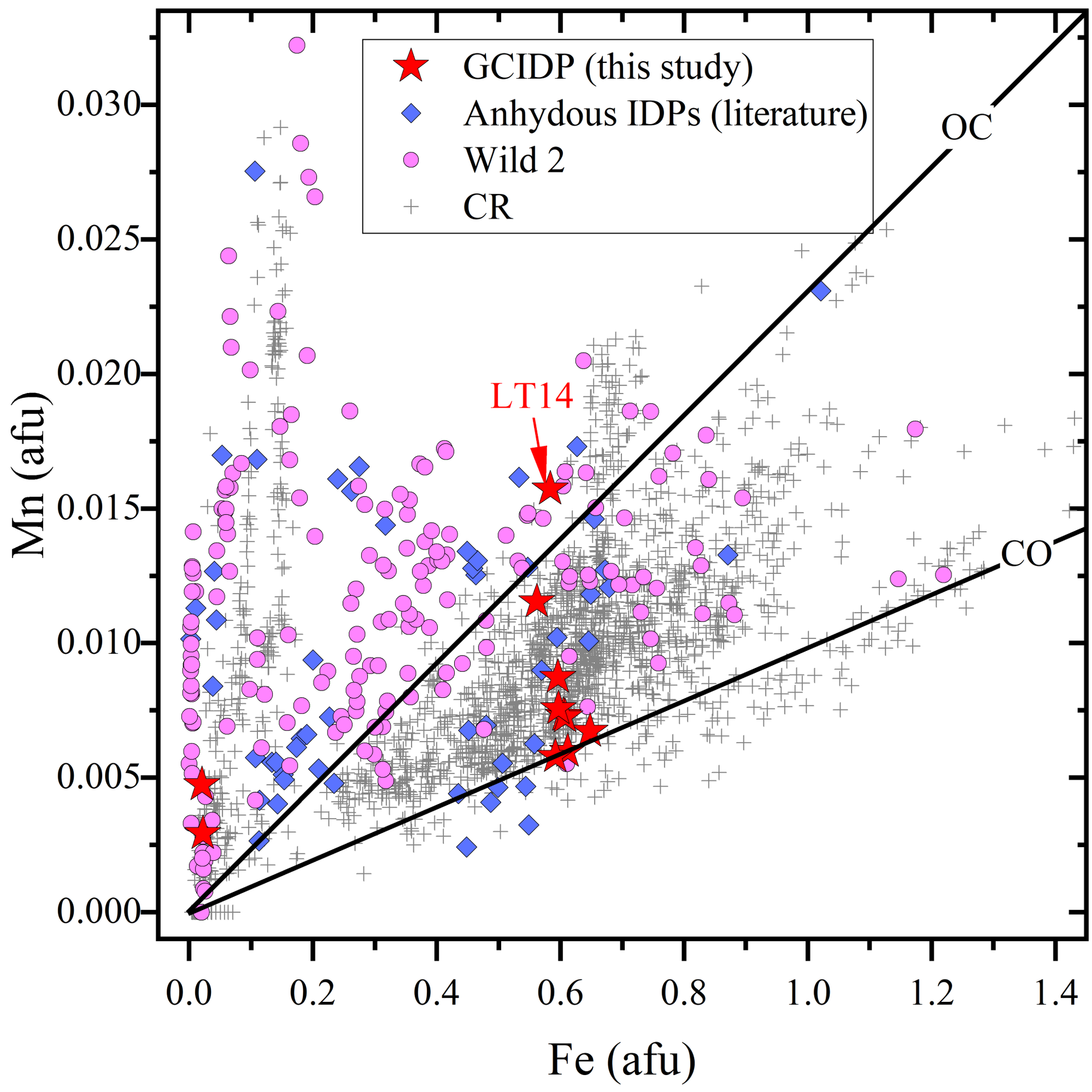
GCIDP (this study)
Anhydous IDPs (literature)
Wild 2
CR
LT14
OC
CO
Mn (afu)
Fe (afu)
0.000
0.005
0.010
0.015
0.020
0.025
0.030
0.0
0.2
0.4
0.6
0.8
1.0
1.2
1.4

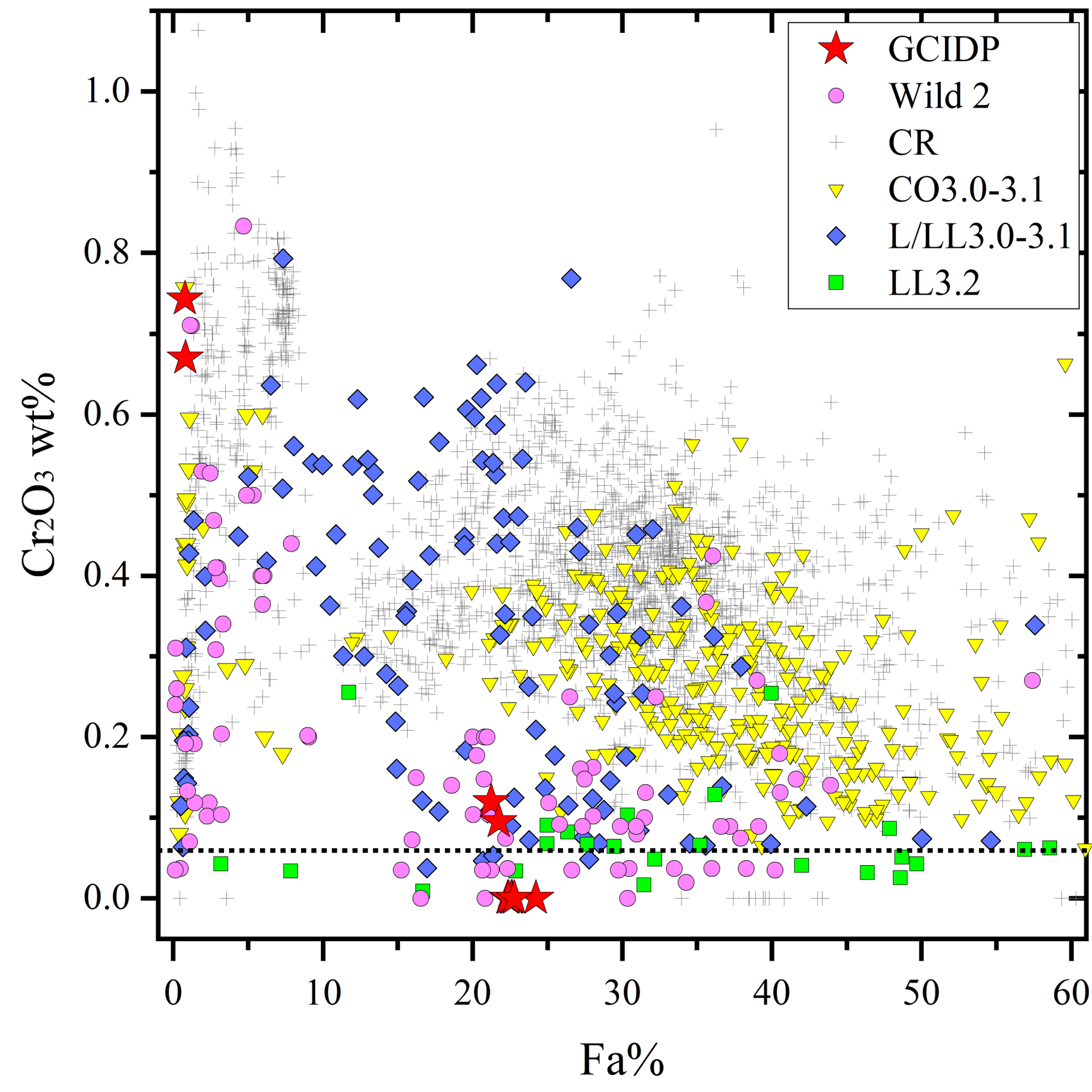
GCIDP
Wild 2
CR
CO3.0-3.1
L/LL3.0-3.1
LL3.2
Cr2O3 wt%
Fa%
0.0
0.2
0.4
0.6
0.8
1.0
0
10
20
30
40
50
60

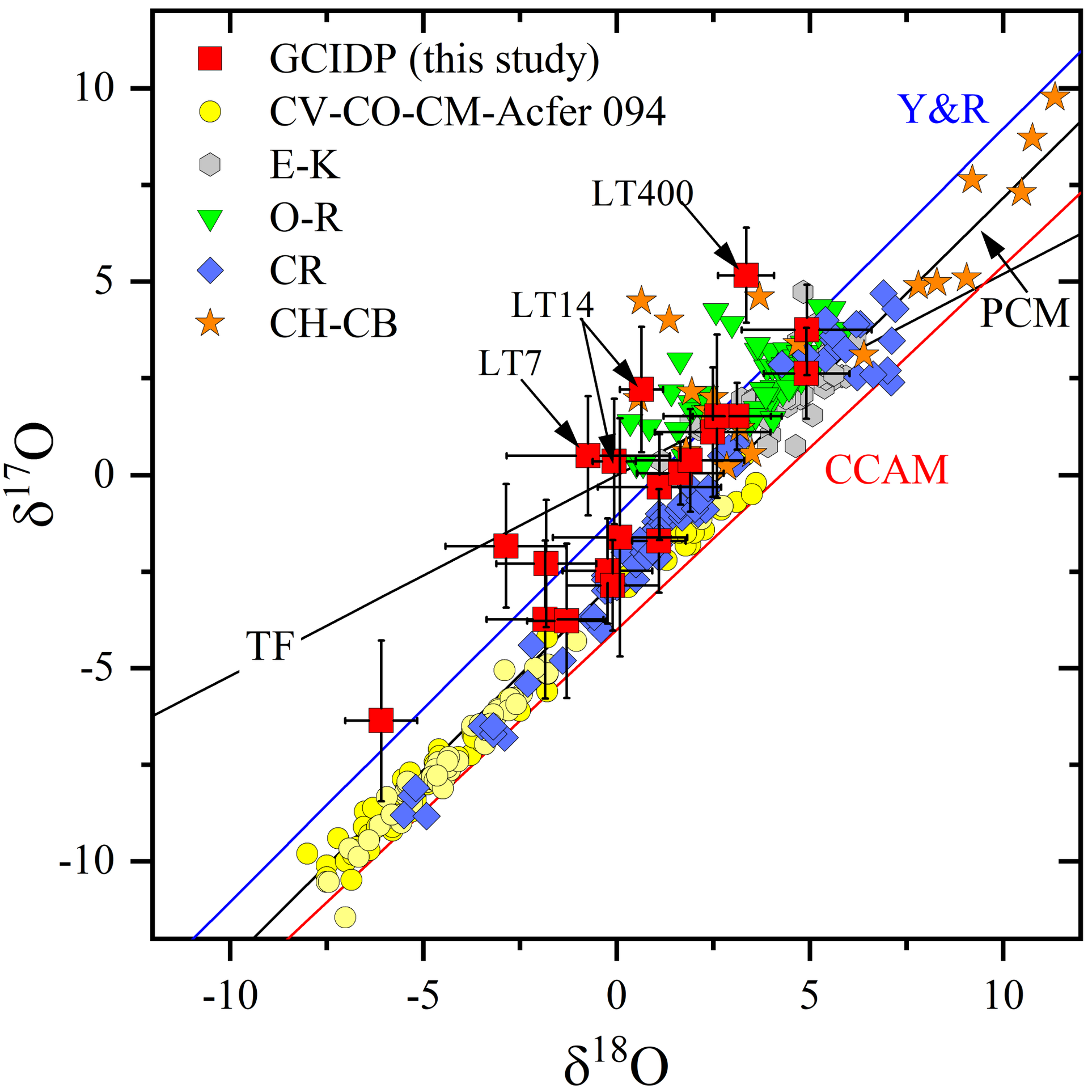
GCIDP (this study)
CV-CO-CM-Acfer 094
E-K
O-R
CR
CH-CB
Y&R
LT400
LT14
LT7
PCM
CCAM
TF
10
5
0
-5
-10
-10
-5
0
5
10
δ17O
δ18O

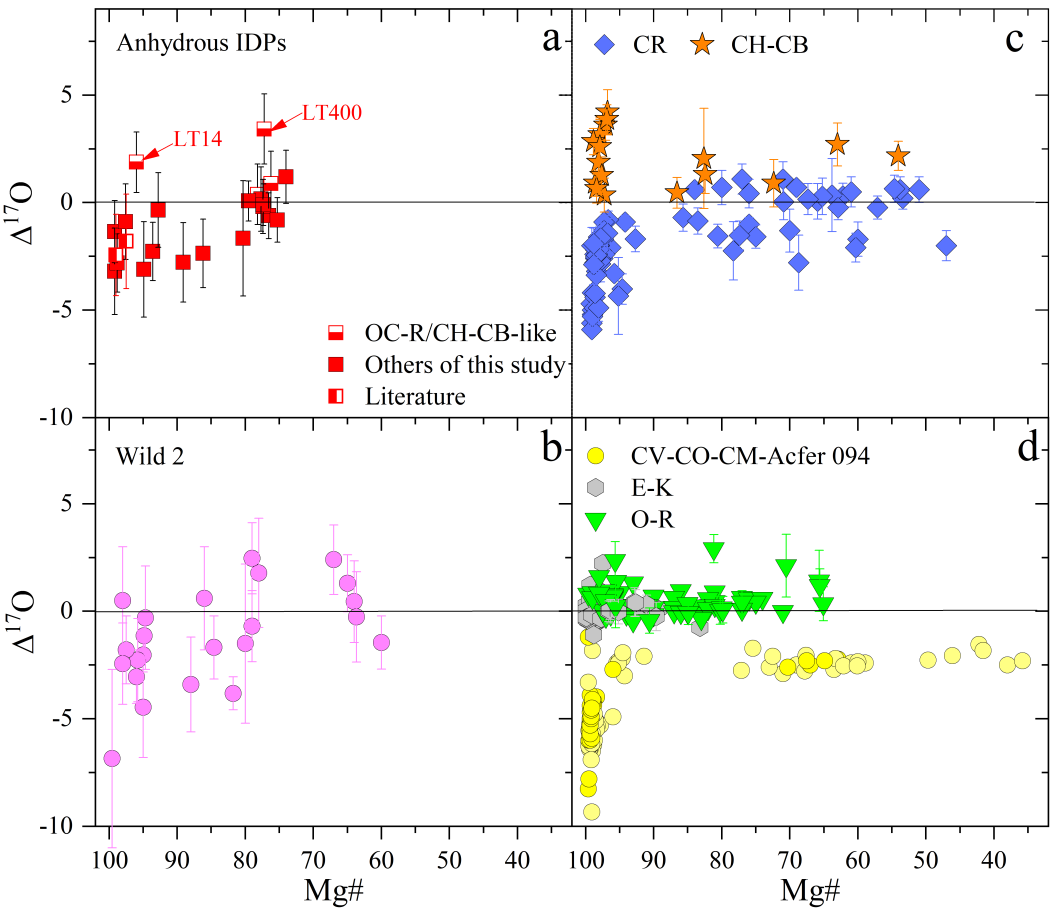
Anhydrous IDPs
a
LT14
LT400
OC-R/CH-CB-like
Others of this study
Literature
CR
CH-CB
c
Wild 2
b
CV-CO-CM-Acfer 094
E-K
O-R
d
Δ17O
Mg#
5
0
-5
-10
100
90
80
70
60
50
40